COVID-19-related drop in anthropogenic aerosol emissions in China and corresponding cloud and climate effects

Axel Timmermann[1,2*], Sun-Seon Lee[1,2], Jung-Eun Chu[1,2],

Eui-seok Chung[1,2], June-Yi Lee[1,2]

[1]Center for Climate Physics, Institute for Basic Science, Busan, South Korea.

[2]Pusan National University, Busan, South Korea

Correspondence should be addressed to: timmermann@pusan.ac.kr

The COVID-19 pandemic has led to massive disruptions of public life on a global scale. To halt the spread of the disease, China temporarily shut down parts of the manufacturing and transportation sectors. Associated anthropogenic aerosol emissions in February 2020 plunged to record lows, causing a temporary improvement of air quality with uncertain effects on cloud formation, atmospheric radiation and climate. To determine the regional and remote climatic impacts of a wide-spread reduction of anthropogenic aerosol emissions in China in early 2020, we conduct a series of sensitivity experiments with a state-of-the art Earth System Model. By reducing February anthropogenic aerosol emissions by 65%, we find evidence for a substantial increase in cloud droplet size and a corresponding enhancement of low cloud cover over Eastern China which intensifies longwave downwelling radiation at the surface but reduces incoming shortwave fluxes, in accordance with observational data. Remote climatic effects of the improvement in air quality can be further identified over the Korean Peninsula and southern Japan. Even though regional climatic responses were only short-lived, the COVID-19-related human interference with earth's radiation balance may hold important clues on how the climate system will respond to the implementation of future long-term air-pollution mitigation strategies.

To contain the spread of the SARS-CoV-2 virus, massive public health interventions were implemented in China[1,2] in February 2020. As a result, large parts of the manufacturing sector

in China halted temporarily, causing a widespread reduction of anthropogenic aerosol emissions after the Chinese New Year holidays. This is illustrated by the rapid ~40-70% drop in atmospheric NO_2 concentrations[3] (**Fig. 1a-c**), Aerosol Optical Depth[4] (**Fig. 1f**) and total CO concentrations[5] (**Fig. 1d**). These changes can be regarded as proxies for an overall slowdown in the sectors of transportation, power and industry[6]. Given, the radiative properties of anthropogenic aerosols[7,8], it is paramount to determine whether lockdown measures in China in February 2020, although only of short duration, may have impacted weather and climate patterns across Eastern Asia.

Previous studies[9] estimated a present-day aerosol direct radiative forcing over China through light absorption and scattering of about -10 W/m^2. Reducing anthropogenic aerosol emissions could hence lead to an increase in surface irradiance[10], subsequent changes in surface air temperature, low level humidity, atmospheric circulation and even shifts in rainfall characteristics[11-13]. Hydrophilic aerosols also serve as cloud condensation and ice nuclei. Their presence therefore increases the concentration of cloud droplets and leads to a reduction of their size. In addition to an associated brightening of the clouds[14] and a resulting reduction of shortwave radiation, aerosols can also change the lifetime and thickness of clouds[15], which may influence radiation properties, the atmospheric circulation, precipitation, and climate in other ways[16,17]. Given the complexity of cloud-aerosol interactions, there are still fundamental uncertainties in quantifying the cloud susceptibility to aerosol changes[18-20] and in determining radiative impacts of aerosols under varying meteorological conditions[16,17]. Resolving such uncertainties is crucial in constraining the future global and regional climate responses to the combination of greenhouse gas and aerosol emissions. Moreover, implementation of future air pollution mitigation strategies – national or international – also requires accurate knowledge of the associated climate impacts. We propose that the unusual situation in February 2020 may serve as a test case to benchmark the performance of state-of-the-art earth system models and their representation of cloud-aerosol interactions in industrialized urban areas.

Whether the climatic anomalies that occurred in February 2020 over parts of East Asia, which included, among others, an increase of low cloud cover (**Fig. 1e**, **Fig. 2d**) over industrialized northeastern China and parts of the Korean Peninsula, decreases in incoming surface shortwave radiation (**Fig. 2e**) and a marked increase in downward surface longwave radiation due to clouds

(**Fig. 2f**), can be directly linked to the imposed reduction of air pollution remains an open question.

The goal of our study is to quantify the effects of reduced regional anthropogenic aerosol emissions over China in February 2020 on the climate system in Eastern Asia. To this end, we conduct a series of 40 idealized simulations with the latest generation NCAR Community Earth System Model[21,22] (CESM) version 2.1.2, with ~1°x1° atmospheric and oceanic resolution. Each model simulation is run for one entire year using observed present-day prescribed anthropogenic aerosol emissions following the Community Emissions Data System[23] scenario (CEDS) for January and from March to December (**Supplementary Fig. 1**). To mimic the effect of the reduced overall industrial activity in February 2020 (**Fig. 1a-f**), 20 of the 40 ensemble members apply strongly reduced (by 65%) February mean anthropogenic aerosol emissions over China north of 26°N (experiment CH35), whereas the other 20 ensemble members use normal present-day values for February from CEDS (experiment CTR). All model simulations are initialized from a coupled model state which is characterized by sea surface temperatures anomalies, that resemble the observations in January 2020 (see Methods) (**Supplementary Fig. 2**). It should be noted here that the overall reduction of anthropogenic aerosol emissions by 65% applied here is an idealized forcing scenario, which ignores the fact that not all aerosol species were affected in the same way by the imposed lock-down measures in February.

In response to the strong reduction of anthropogenic aerosol emissions over China, the ensemble mean of the CH35 simulations exhibits a strong and statistically significant (i.e. the null hypothesis of equal means can be rejected beyond the 95% confidence level) regional increase in low cloud coverage (**Fig. 2a**). The strongest regional signals are co-located with the anomalies in surface aerosol fluxes (**Supplementary Fig. 3**) and aerosol optical depth (**Supplementary Fig. 4a**). As a result of synoptic atmospheric variability, however, the negative air pollution anomalies and associated cloud changes also extend far beyond the forcing region (**Fig. 2a**). A similar low cloud response, albeit stronger and shifted somewhat to the north, can be seen in the observations (**Figs. 1e, 2d**). Please note that the model statistics represents an ensemble mean over 20 members, which emphasizes the forced signal. In contrast, the observations represent only one single trajectory which more affected by synoptic, unforced, atmospheric conditions. Thus, we expect the observations to show a lower forced signal to internal noise ratio compared to the model analysis.

The enhanced low cloud cover over northeastern China in both model and the observations reduces the amount of sunlight at the surface (**Fig. 2 b, e**) by ~10-15 W/m^2. This cooling tendency is partly offset (~3-10 W/m^2) by a positive anomaly in the downwelling longwave radiation (**Fig. 2 c, f**), which can be partly explained by the longwave-absorbing and scattering properties of clouds[24,25]. To understand the seemingly counter-intuitive result that an overall reduction of hydrophilic aerosols in CH35, which would normally serve as cloud condensation nuclei (**Fig. 3a**) generates an increase in low cloud cover over China (**Fig. 2a, 3b)**, one needs to consider the effect of cloud droplet size. As a result of reduced anthropogenic aerosols concentration in CH35, the simulated cloud droplet size over China (averaged over 105°E-120°E, 30°N-35°N) increases considerably from the surface to the lower atmosphere (**Fig. 3c**) from about 1.65 ± 0.55 micron at 760 hPa to about 2 ± 0.55 micron. A statistically significant (95% confidence) increase in simulated cloud droplet size translates into reduced droplet evaporation (smaller surface area) and increased chance for precipitation (**Fig. 4a**). Increased condensation and precipitation release heat to the surrounding air, enhancing lower tropospheric static stability and trapping moisture in the lower atmosphere. This process increases relative humidity which further promotes the formation of low clouds and fog (**Fig. 3d, Supplementary Fig. 4c**). The simulated lowering of the condensation level and hence of the stratus cloud base height relative to the polluted conditions is in good qualitative agreement with the observed anomalies in February 2020 (**Fig. 1e, 2d**) and previous field campaigns conducted over Wuhan[26].

The CESM simulations also show a response over the Korean Peninsula, which is characterized by reduced concentration of cloud condensation nuclei (**Supplementary Fig. 5a**) and a statistically significant (more than 95% confidence) increase of middle tropospheric clouds (**Supplementary Fig. 4d, Supplementary Fig. 5b**) with corresponding shifts in mid-troposphere-level relative humidity (**Supplementary Fig. 5d**). These changes are accompanied by an increase of longwave cloud forcing over the Korean Peninsula (**Fig. 2c**), which can further contribute to the surface warming tendency (**Fig. 4b**).

The ensemble mean response shows a weak cooling of about ~0.3°C over the central part of eastern China (**Fig. 4b**), and some warming around it and across the Korean Peninsula. Overall however, the simulated surface temperature changes over this area 110°E-120°E 30°-35°N are statistically insignificant. In contrast, the observed surface air temperature anomalies in February 2020 (relative to the years 2016-2019) are characterized by a massive warming (**Fig. 4d**), in the low elevation areas of Eastern China, the Korean Peninsula and Japan attaining values of up to

4°C. The discrepancy between model response and observed changes further highlights the importance of lateral heat advection associated with synoptic-scale (unforced) atmospheric variability, which we suppress in the ensemble mean statistics to highlight the forced signal.

Aerosol-cloud interactions can also have a discernable impact on the hydrological cycle and rainfall characteristics[13]. CH35 simulates an increase of precipitation just to the east of the largest anomaly in low cloud cover in northeastern China (statistically significant beyond 95%), which extends further across South Korea (**Fig. 4a**). The precipitation pattern also aligns well with the cloud longwave forcing (**Fig. 2c**), which indicates that the downwelling longwave cloud radiative forcing may be partly driven by the release of latent heat and the warming of the lower atmospheric layers during the precipitation process. The total precipitation changes in the observations (**Fig. 4c**) resemble the simulated anomalies (**Fig. 4a**), in particular over the Shandong and Hebei provinces and the Beijing and Tianjin municipalities. The reanalysis dataset also shows a close correspondence between precipitation and longwave cloud radiative forcing anomalies (**Fig. 2f**) during the February 2020 period, which suggests that the CESM model experiments capture essential aerosol-cloud-precipitation processes realistically.

Summarizing, our study demonstrated that public health interventions and a resulting temporary reduction of industrial activities over China in February 2020 – a response to the COVID-19 outbreak – had a discernable climatic effect over China and the neighboring Korean Peninsula. By running a 20-member ensemble of anthropogenic aerosol emission sensitivity experiments, we were able to distinguish the forced response from the internal atmospheric noise. The forced signal of an increased low-level cloud cover and increased precipitation in February (**Figs. 2a, 4a, c, Supplementary Fig. 6**) is qualitatively consistent with the observations (**Fig. 1e, Fig. 2d-f**).

With other countries imposing similar lock-down measures to battle the spread of the COVID-19 disease, air quality also improved elsewhere, at least temporarily. The methods applied here could be further used to ascertain the climatic influences of the 2020 pandemic on India, the United States and Europe. The atmospheric data collected during such periods of rapid and constrained anthropogenic radiative perturbations may become an invaluable resource to test and calibrate climate and atmospheric chemistry models, which in turn will help in determining the impacts of future long-term air pollution mitigation strategies on our climate system. Moreover, the regional and temporary anthropogenic aerosol reductions that have occurred and may

continue to occur over the coming months in other parts of our planet may provide important data to learn more about cloud-aerosol-precipitation-climate interactions[16], which still remain one of the largest uncertainties in future climate change assessments.

Author contributions A.T. designed the study, conducted data analysis and prepared figures. S.-S. Lee and J.E Chu developed the forcing files, conducted the CESM2.1.2 simulations and statistical data analysis and prepared figures. E.-S. Chung analysed the satellite and ERA5 data. All authors contributed to writing the manuscript.
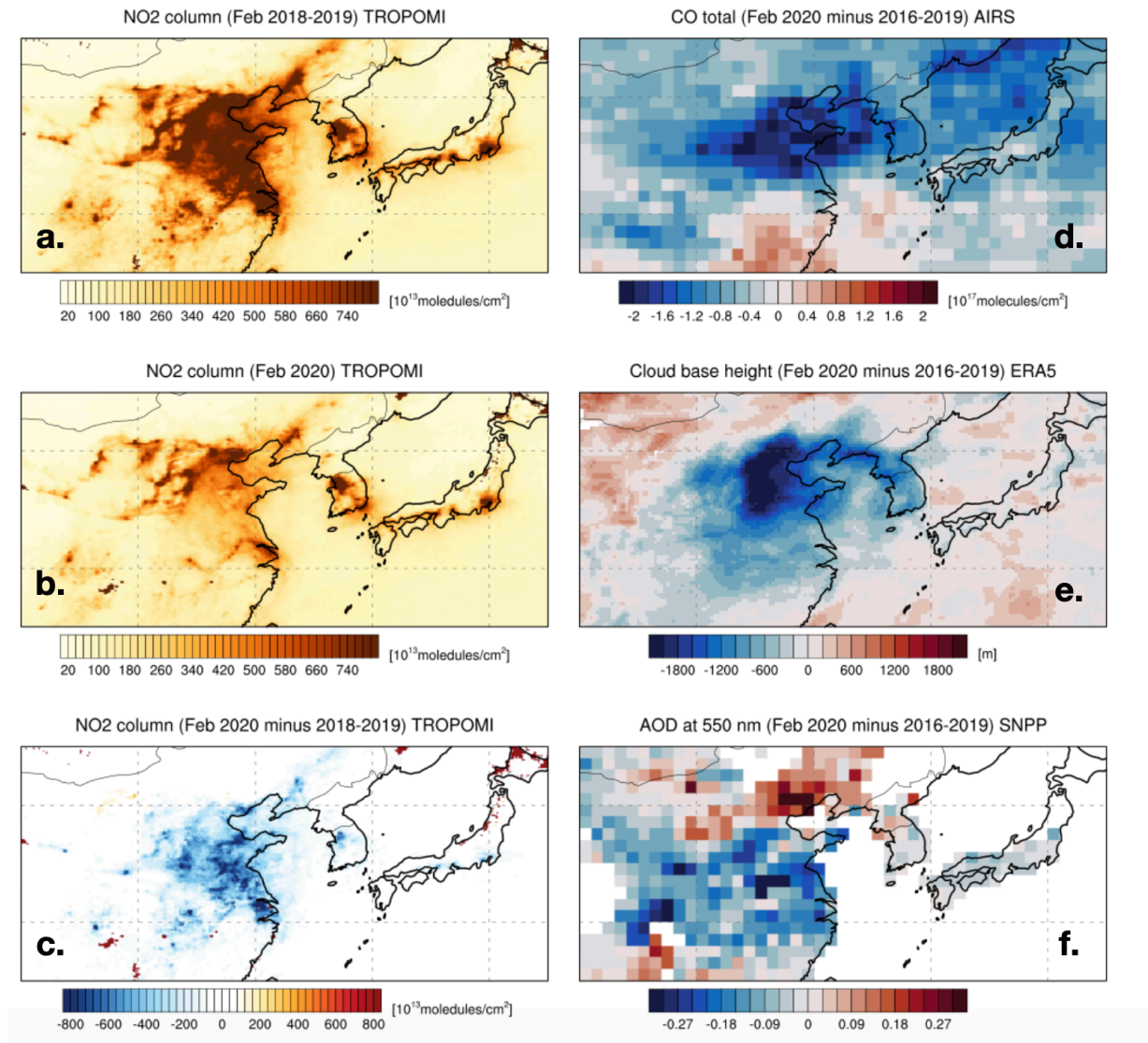
Fig. 1 February 2020 reduction of air pollution over China and cloud response: a. February monthly mean of near-surface NO_2 concentrations averaged from 2018 and 2019 in [10^{13} molecules/cm^2]. Data from TROPOMI[3] version 1.0; b. same as a., but for February 2020; c. Difference between b. and a.; d. Difference of total carbon monoxide concentration [10^{17} molecules/cm^2] for February 2020 minus the February composite over years 2016-2019 from AIRS[5] (Atmospheric Infrared Sounder)/Aqua L3; e. Difference of monthly low cloud base height [m] for February 2020 minus the February composite over years 2016-2019 from ERA5[27]; f. Difference of Aerosol Optical Depth at 550 nm for February 2020 minus February composite over years 2016-2019 using Suomi National Polar-orbiting Partnership (SNPP) Visible and Infrared Imaging Radiometer Suite (VIIRS) NASA standard Level-3 monthly deep blue aerosol data[4].
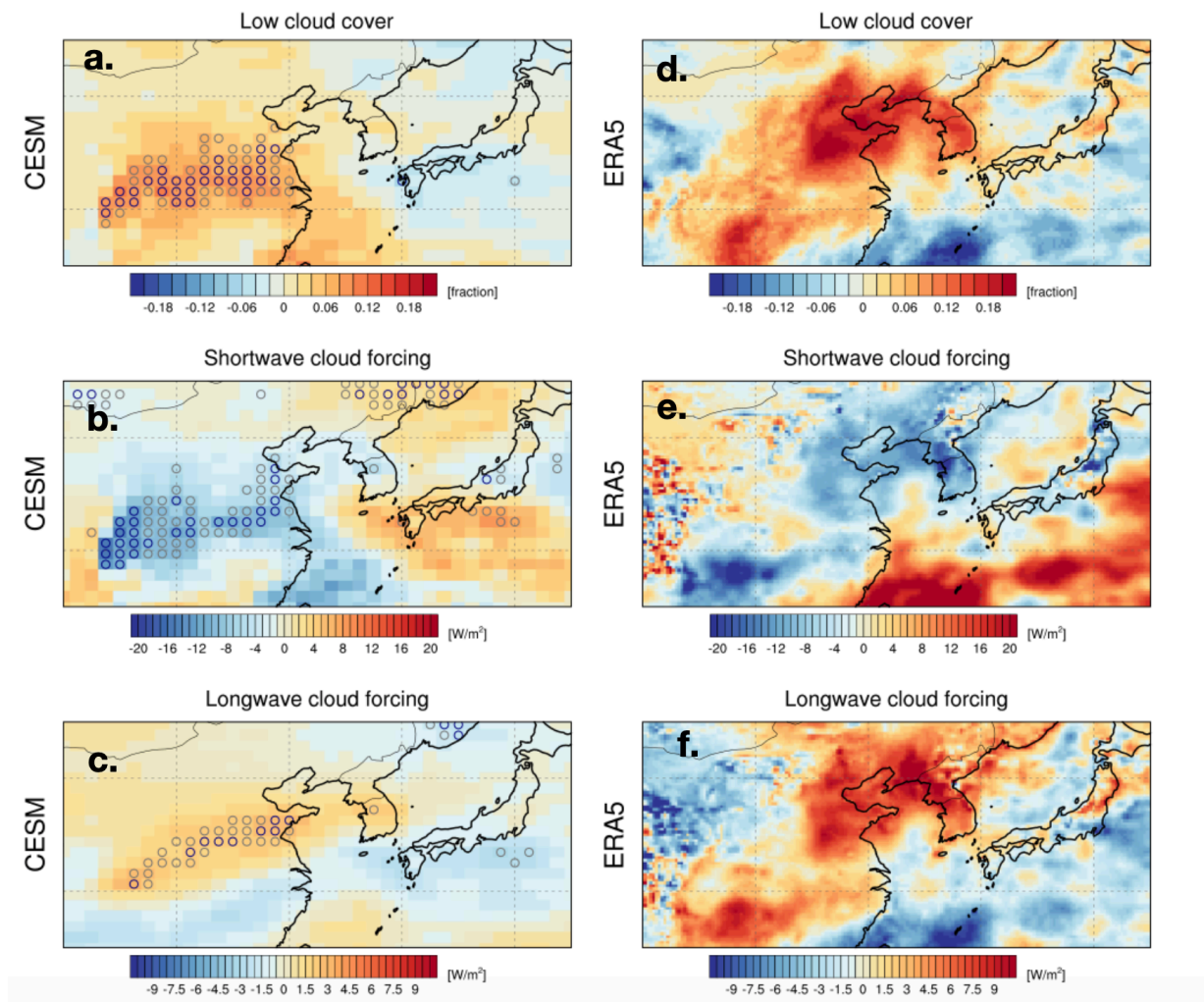
Fig. 2 Cloud response to anthropogenic aerosol reduction over China: a. Ensemble mean difference of monthly vertically integrated low cloud cover in February between CH35 and CTR simulations; b., same as a., but for shortwave cloud forcing [W/m²]; c., same as a., but for longwave cloud forcing [W/m²]; d. difference of low cloud cover between February 2020 and the February composite over years 2016-2019 from ERA5[27]; e. same as d. but for surface shortwave cloud radiative forcing [W/m²].; f. same as d. but for surface longwave cloud forcing [W/m²]. Grid points for which the CTR and CH35 simulations have significantly different mean values are highlighted by gray (navy) colored circles, representing the 90% (95%) confidence ranges.
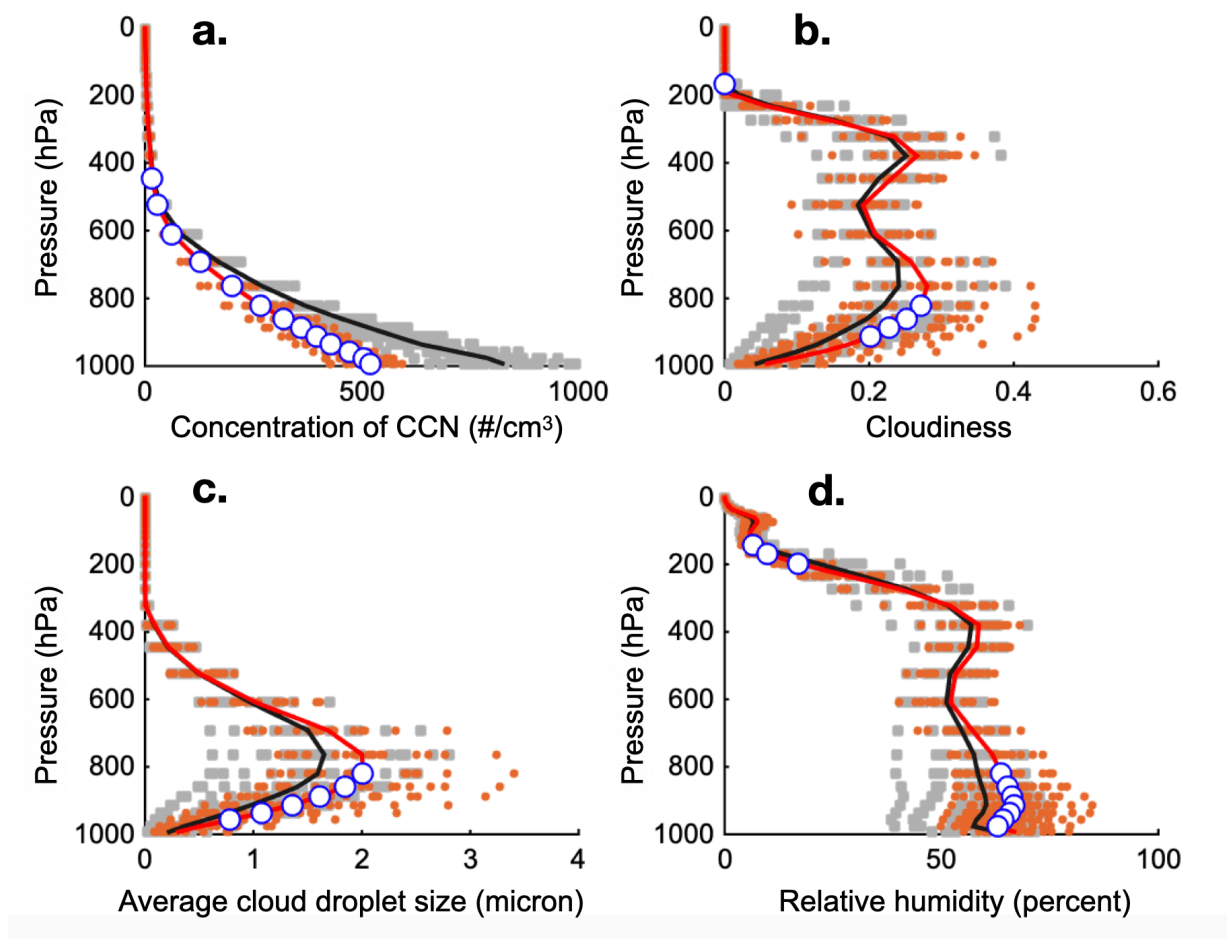
Fig. 3 Effect of anthropogenic aerosol reduction on cloud properties over China: a. Cloud condensation nuclei concentration as function of pressure in February averaged over China (105ºE-120ºE 30ºN-35ºN) for the CTR simulation (20 members, gray squares, ensemble mean black line) and the CH35 simulation with reduced anthropogenic aerosol forcing over China (20 members, orange circles, ensemble mean red line, blue circles indicate statistically significant changes, more than 95% confidence in rejecting null hypothesis of equal means between CTR and CH35); b., same as a., but for cloudiness; c., same as a., but for average droplet effective radius; d., same as a., but for relative humidity.
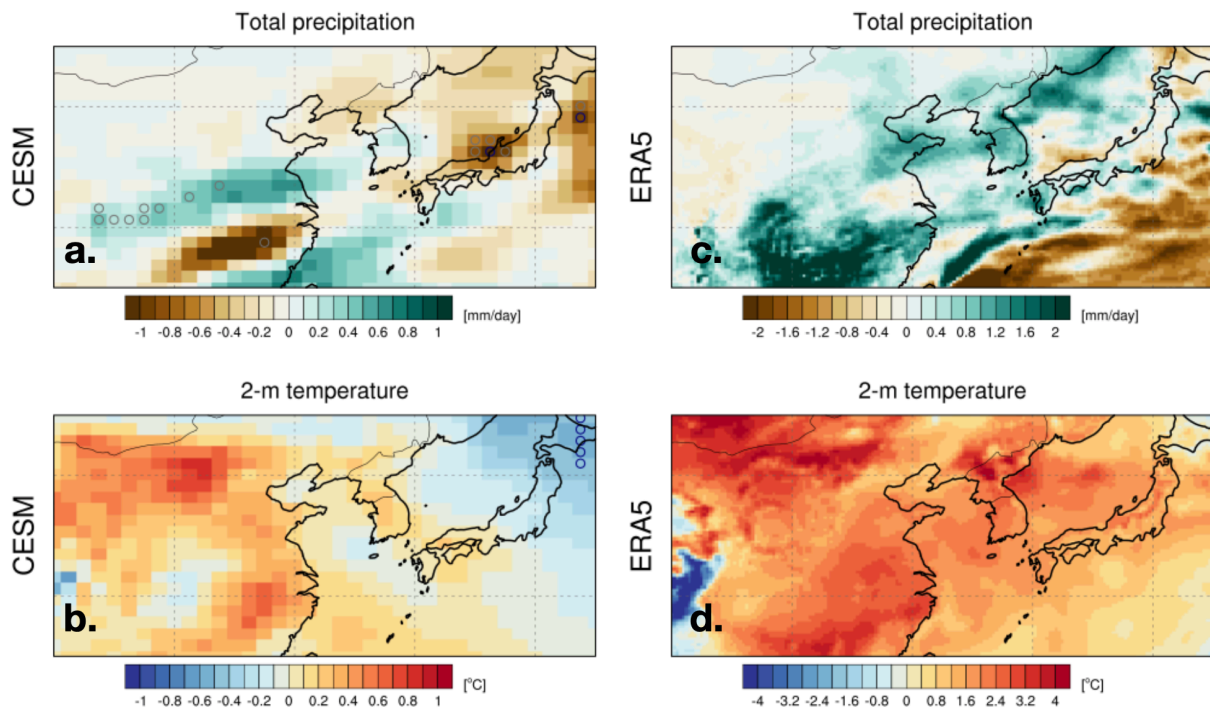
Fig. 4 Climate anomalies occurring during period of reduced aerosol emissions in climate model and observations: a. Difference of monthly total precipitation [m/s] in February between CH35 and CTR simulation averaged over 20 ensemble members; b., same as a., but for surface air temperature; c. difference of precipitation [m/s] between February 2020 and the February composite over years 2016-2019 from ERA5[27]; d., same as c., but for surface air temperature (note the different color bar range in b. and d). Grid points for which the CTR and CH35 simulations have significantly different mean values are highlighted by gray (navy) colored circles, representing the 90% (95%) confidence range.

METHODS

Community Earth System Model, version 2.1.2

Our model experiments are based on the NCAR Community Earth System Model[21,22], version 2.1.2, with ~1°x1° atmospheric and oceanic resolution. We conduct a 20-member ensemble of 1-year-long simulations in which all anthropogenic emissions over China (north of 26°N) are scaled down in February to 35% (CH35) (**Supplementary Fig. 1**). The reduction lasts for 1 month, starting from February 1st and is applied to the emissions of a number of anthropogenic aerosols, originating from energy, industry, residential, transportation, agriculture and waste sectors CEDS[23,28]. The resulting changes in surface aerosol fluxes are depicted for some exemplary aerosols (Particulate Organic Matter, SO_2, SO_4, and Black Carbon) in **Supplementary Fig. 3**.

Each experiment is repeated 20 times using slightly different atmospheric initial conditions (micro-perturbations) to better identify the forced response from natural short-term variability (**Supplementary Fig. 1)**. The simulation length per ensemble member is 12 months (January 1st, - December 31st), even though our analysis only focuses on February conditions. The experiments were initialized from an initial condition obtained from a 60-year present-day control simulation, for which the simulated sea surface temperature anomaly (SSTA) resembles the observed January 2020 SSTA (**Supplementary Fig. 2**) in terms of spatial deviations from the global mean. The CH35 simulations are then compared to a 20-member micro-perturbation control ensemble, which is initialized from the same January 2020 SSTA state, but which applies the standard February model anthropogenic aerosol emissions[23,28] without reduction over China.

### Extraction of realistic initial conditions

To further constrain our CESM2.1.2 simulations to the observations, we selected sea surface temperature anomaly (SSTA) initial conditions from a 60-year-long present-day simulation with cyclic 2010 anthropogenic aerosol emissions and greenhouse gas concentrations, that bear a optimal resemblance to the observed SSTA field in January 2020 from HadISST[29] and ERSST[30] datasets (**Supplementary Fig. 2**). The initial conditions were obtained by minimizing the root mean squared error (rmse) between the observed January 2020 SST anomalies (minus the spatial mean value from 60°S-60°N) and the simulated values (for each January of the 60-year simulation). The model simulation year with the lowest rmse relative to

the observed January 2020 conditions (**Supplementary Fig. 2**) was then selected as initial condition for the 40-member ensemble sensitivity experiments CTR and CH35.
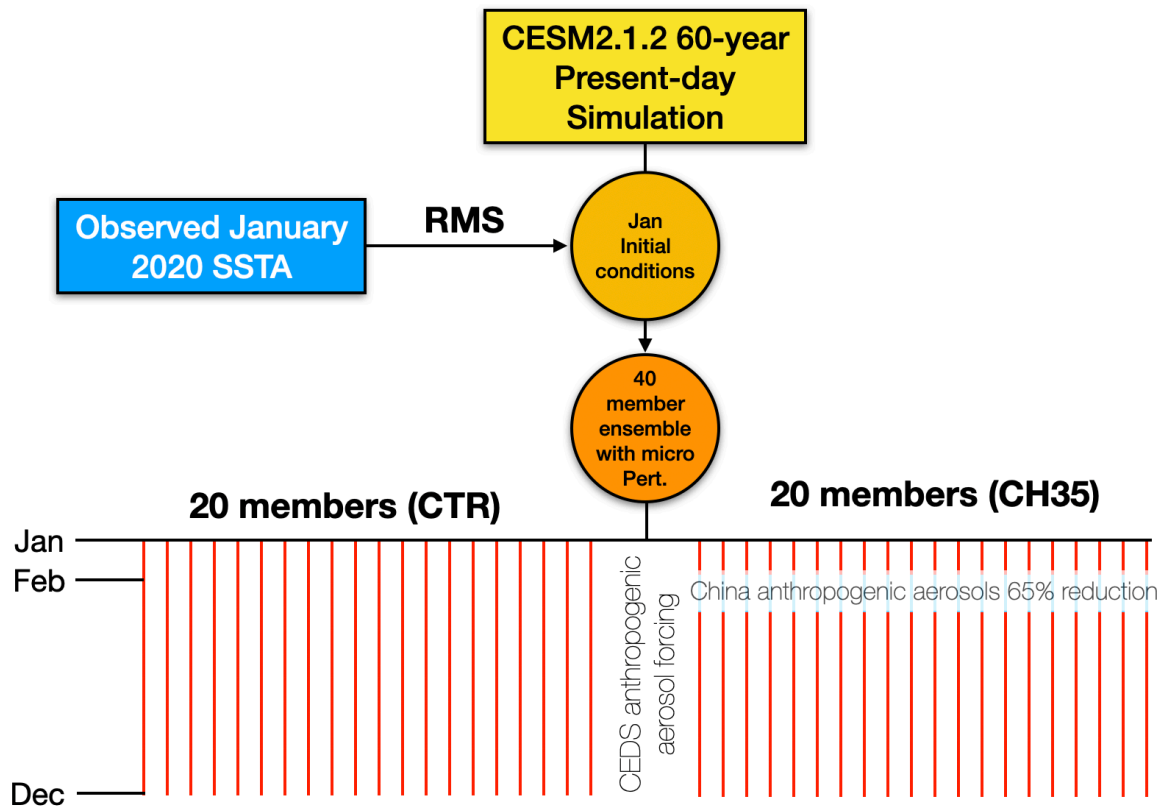
Supplementary Fig. 1, **Schematic of experimental design.** Optimal initial conditions are extracted from a 60-year-long present-day simulation conducted with CESM2.1.2, using the perpetual anthropogenic aerosol emissions[23,28] from 2010. A 20-member ensemble is conducted (with micro-perturbations in the atmospheric state) from the optimal initial conditions using 2010 aerosol forcing (CTR). Another 20-member ensemble uses 2010 anthropogenic aerosol emissions, except for February, when the emissions are reduced by 65% in China north of 26°N (CH35). This set of experiments mimics the slow-down of the energy, transportation and industry sectors in February 2020 – a result of public health interventions to curb the spread of COVID-19.
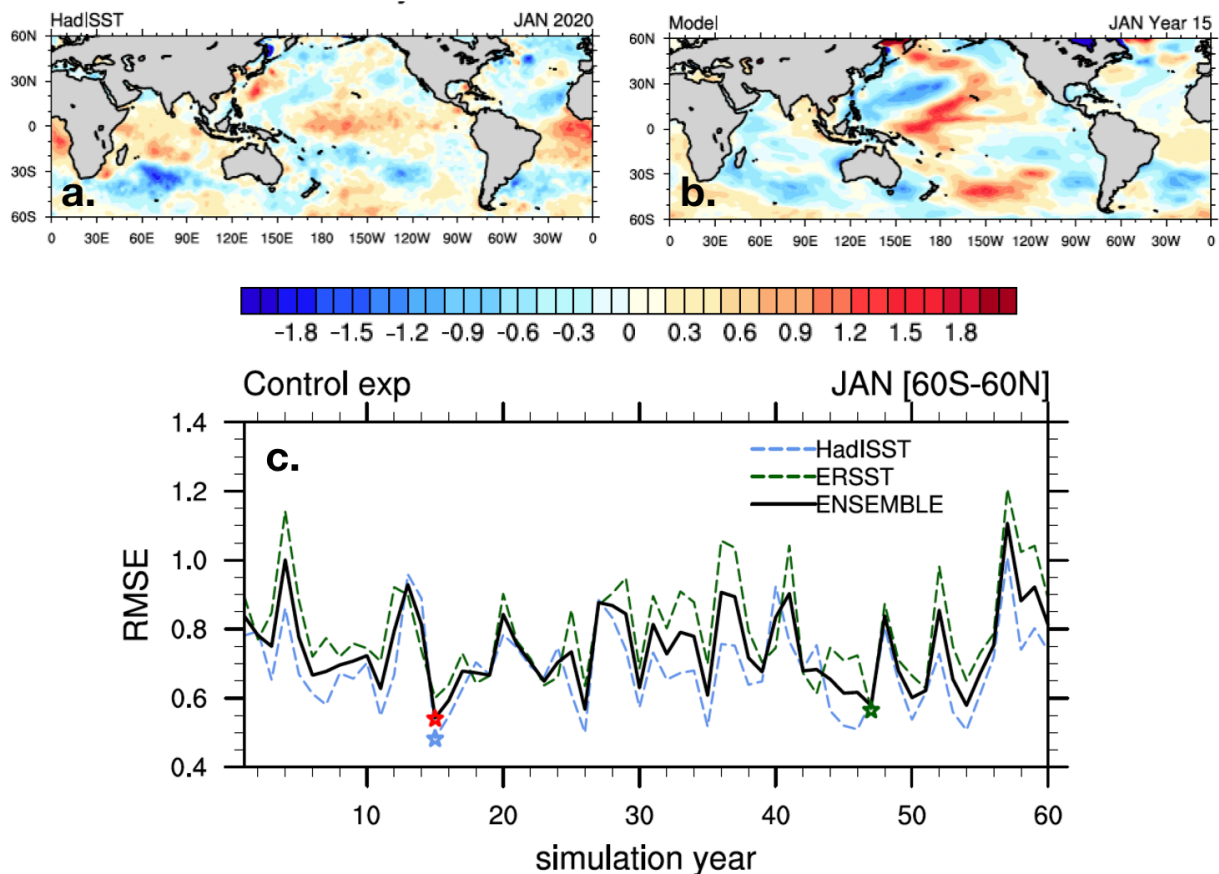
Supplementary Fig. 2, **Identification of initial conditions for CESM2.1.2 experiments.** a. observed monthly sea surface temperature anomalies (SSTA) [°C] (minus spatial mean from 90°S-90°N) for January 2020 from HadISST[29]; b. Simulated SSTA with the highest similarity (in terms of root mean squared error) from a. obtained from 60-year-long present-day control simulation; c. spatial root mean squared error ([°C]) (rmse) between SSTA field from 60-year-long present-day control simulation and January 2020 SSTA conditions from HadISST[29] (see a) (blue dashed) and from ERSST dataset[30] (green dashed line) and mean of rmse timeseries (black line). The years of minimum rmse from HadISST, ERSST and the averaged rmse between HadISST and ERSST (ENSEMBLE) are marked as red, green, and blue stars, respectively.
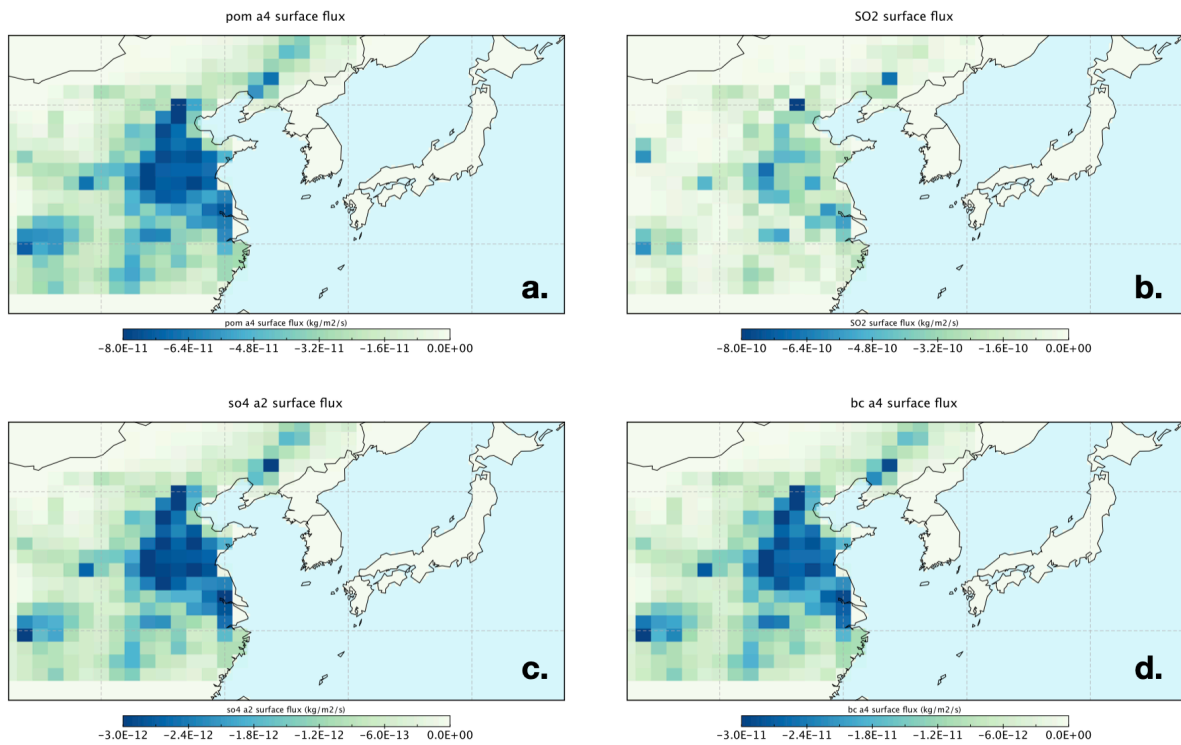
Supplementary Fig. 3, **Map of anthropogenic February aerosol surface flux anomalies in CESM2.1.2 simulation:** Simulated February monthly mean flux anomaly (CH35 minus CTR) for a. Particulate Organic Matter (a4 size class) (kg/m²/s); b. SO_2 flux (kg/m²/s); c. SO_4 (a2 size class) flux (kg/m²/s); d. black carbon (a4 size class) (kg/m²/s).
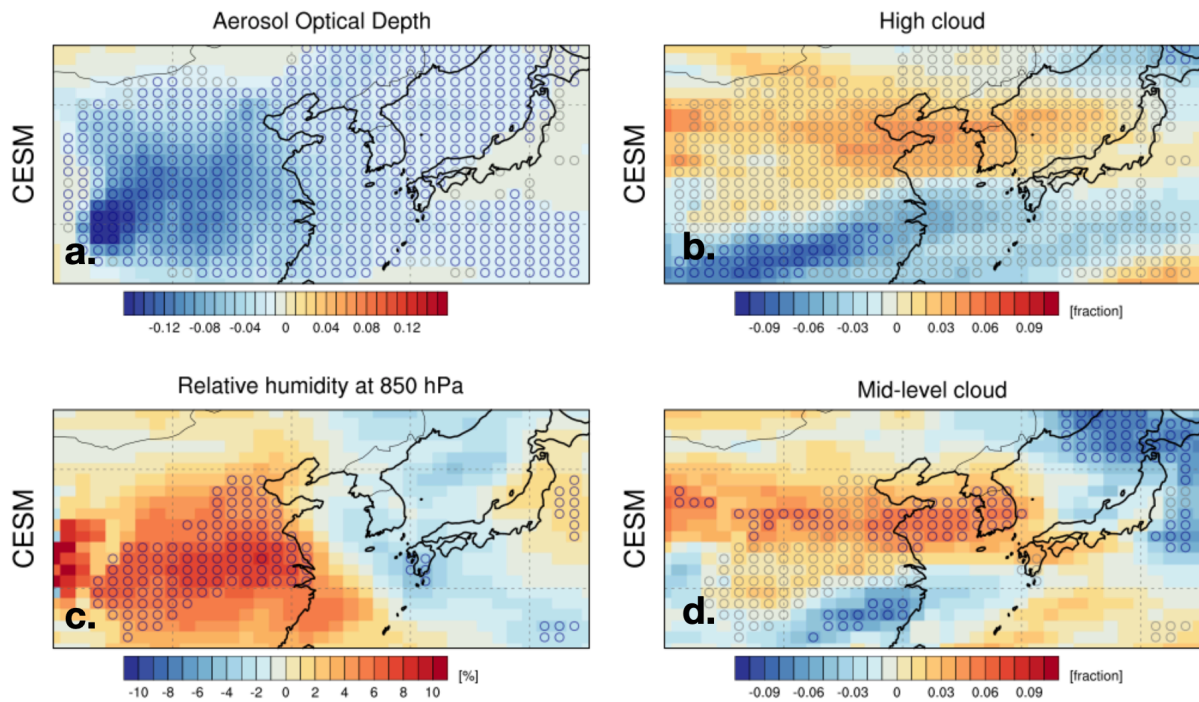
Supplementary Fig. 4 Atmospheric response to reduced aerosol emissions in CH35: Difference of aerosol optical depth in February between CH35 and CTR simulation averaged over 20 ensemble members; b., same as a., but for high cloud cover; c., same as a., but for relative humidity at 850 hPa (percent); d. same as a., but for medium-level cloud cover; gray (navy) circles indicate grid points for which the null hypothesis of equal means of CTR and CH35 can be rejected at the 90 (95%) confidence level.
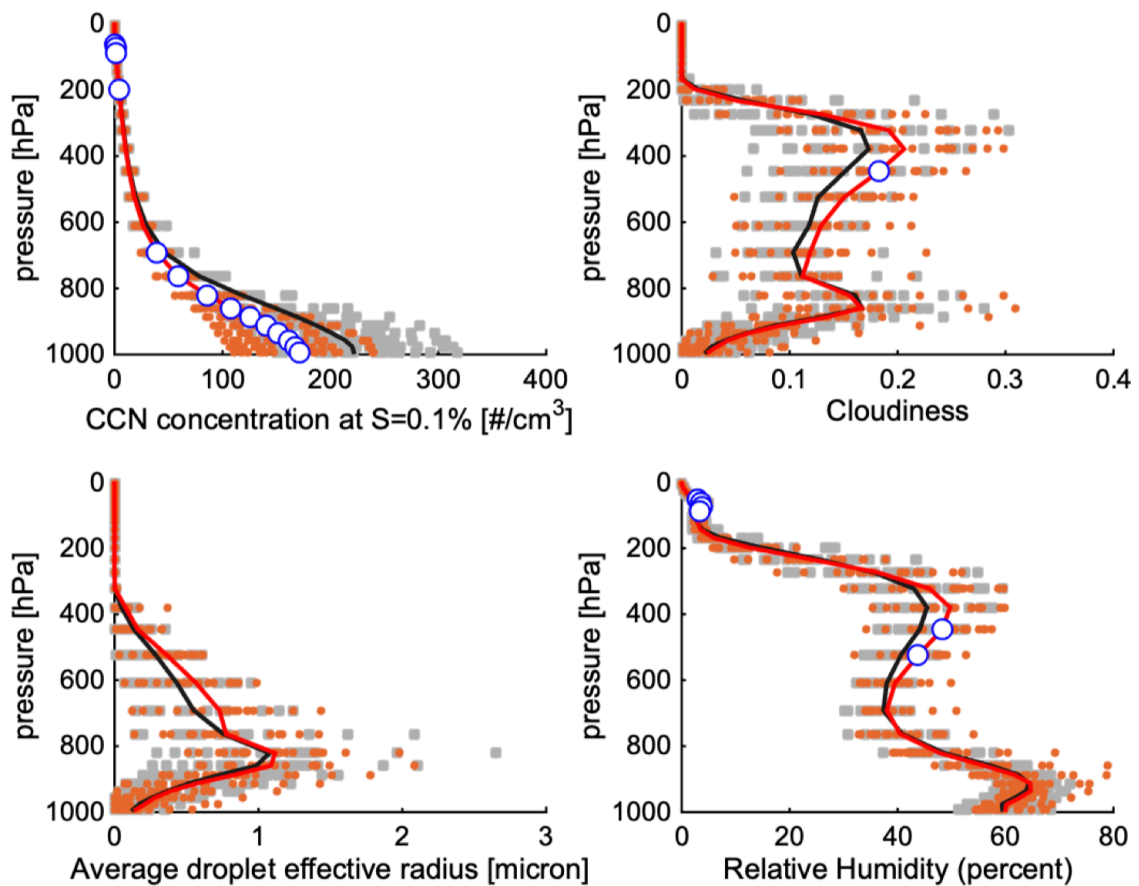
Supplementary Fig. 5 Effect of anthropogenic aerosol reduction on cloud properties over Korean Peninsula: a. Cloud condensation nuclei concentration as function of pressure in February averaged over Korea (125ºE-130ºE 35ºN-40ºN) for the CTR simulation (20 members, gray squares, ensemble mean black line) and the CH35 simulation with reduced anthropogenic aerosol forcing over China (20 members, orange circles, ensemble mean red line, blue circles indicate statistically significant changes, i.e. the null hypothesis of equal means can be rejected at the 95% confidence level); b., same as a., but for cloudiness; c., same as a., but for average droplet effective radius; d., same as a., but for relative humidity.
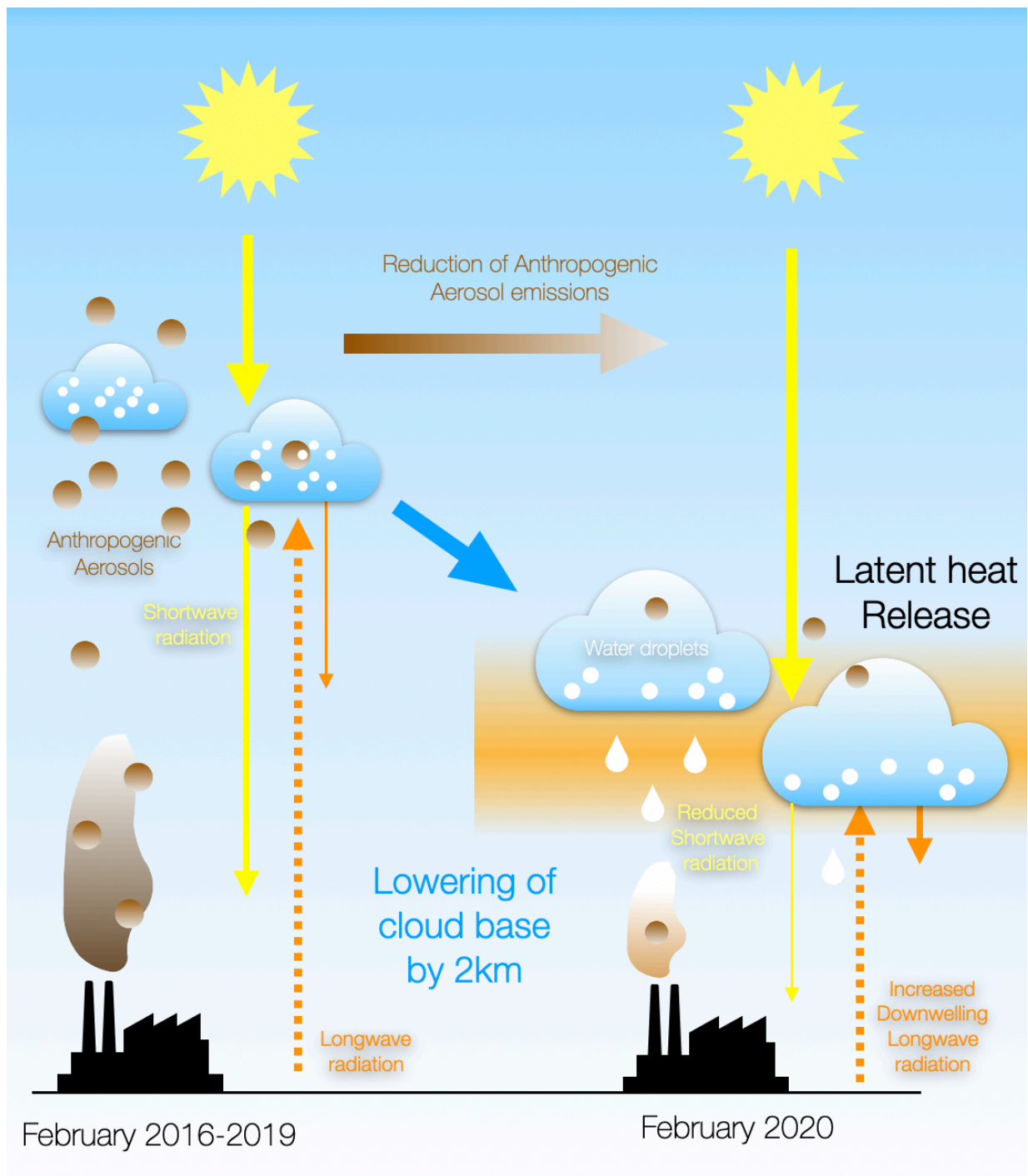
Supplementary Fig. 6, **Schematic of observational and simulated changes in cloud properties over northeastern China**. In February 2020, the cloud base over Eastern China dropped by 2 km (Fig. 1e) which also increased the chances for the occurrence of fog. This feature was caused by the reduction of anthropogenic aerosols and the resulting increased cloud droplet size. Both model simulations and observations show slightly increased precipitation over Shandong and Hebei provinces and the Tianjin and Beijing municipalities and stronger downwelling longwave radiation and a decreased shortwave radiation. The increased precipitation from low-level clouds increased the latent heat release, causing warming and

This is a non-peer reviewed preprint submitted to EarthArXiv

increased static stability of the lower atmosphere. This can further contribute to the trapping more moisture in the lower levels, thereby promoting the formation of clouds.

REFERENCES

[1] B. Salzberger, T. Gluck, and B. Ehrenstein, Infection.
[2] F. H. Gong, Y. Xiong, J. Xiao, L. Lin, X. D. Liu, D. Z. Wang, and X. K. Li, Frontiers of Medicine.
[3] J. H. G. M. van Geffen, H. J. Eskes, K. F. Boersma, J. D. Maasakkers, and J. P. Veefkind, in *Report S5P-KNMI-L2-0005-RP* (KNMI, De Bilt, The Netherlands, 2019).
[4] A. M. Sayer, N. C. Hsu, J. Lee, C. Bettenhausen, W. V. Kim, and A. Smirnov, Journal of Geophysical Research-Atmospheres **123**, 380 (2018).
[5] J. Susskind, J. M. Blaisdell, and L. Iredell, Journal of Applied Remote Sensing **8**, 084994 (2014).
[6] M. Li *et al.*, Atmospheric Chemistry and Physics **17**, 935 (2017).
[7] M. Schulz *et al.*, Atmospheric Chemistry and Physics **6**, 5225 (2006).
[8] D. T. Shindell *et al.*, Atmospheric Chemistry and Physics **13**, 2939 (2013).
[9] B. L. Zhuang, S. Li, T. J. Wang, J. J. Deng, M. Xie, C. Q. Yin, and J. L. Zhu, Atmospheric Environment **79**, 349 (2013).
[10] F. Liang and X. A. Xia, Annales Geophysicae **23**, 2425 (2005).
[11] S. Liu, J. Xing, B. Zhao, J. D. Wang, S. X. Wang, X. Y. Zhang, and A. J. Ding, Current Pollution Reports **5**, 36 (2019).
[12] C. X. Li, T. B. Zhao, and K. R. Ying, Theoretical and Applied Climatology **125**, 529 (2016).
[13] D. Rosenfeld, U. Lohmann, G. B. Raga, C. D. O'Dowd, M. Kulmala, S. Fuzzi, A. Reissell, and M. O. Andreae, Science **321**, 1309 (2008).
[14] S. Twomey, Atmospheric Environment **8**, 1251 (1974).
[15] B. A. Albrecht, Science **245**, 1227 (1989).
[16] B. Stevens and G. Feingold, Nature **461**, 607 (2009).
[17] D. Rosenfeld, S. Sherwood, R. Wood, and L. Donner, Science **343**, 379 (2014).
[18] T. Michibata, K. Suzuki, Y. Sato, and T. Takemura, Atmospheric Chemistry and Physics **16**, 15413 (2016).
[19] Y. Sato, D. Goto, T. Michibata, K. Suzuki, T. Takemura, H. Tomita, and T. Nakajima, Nature Communications **9**, 985 (2018).
[20] V. Toll, M. Christensen, J. Quaas, and N. Bellouin, Nature **572**, 51 (2019).
[21] A. Gettelman *et al.*, Geophysical Research Letters **46**, 8329 (2019).
[22] G. Danabasoglu *et al.*, Journal of Advances in Modeling Earth Systems **12**, e2019MS001916 (2020).
[23] R. M. Hoesly *et al.*, Geoscientific Model Development **11**, 369 (2018).
[24] A. Arking, Bulletin of the American Meteorological Society **72**, 795 (1991).
[25] D. L. Hartmann and D. Doelling, Journal of Geophysical Research-Atmospheres **96**, 869 (1991).
[26] W. Wang, T. H. Zhang, and Z. X. Pan, Atmospheric Pollution Research **10**, 1531 (2019).

[27]   C. C. C. S. (C3S), Copernicus Climate Change Service Climate Data Store (CDS), M*arch 1st, 2020.*, 2017).

[28]   L. Y. Feng *et al.*, Geoscientific Model Development **13**, 461 (2020).

[29]   N. A. Rayner, D. E. Parker, E. B. Horton, C. K. Folland, L. V. Alexander, D. P. Rowell, E. C. Kent, and A. Kaplan, Journal of Geophysical Research-Atmospheres **108**, 4407 (2003).

[30]   R. W. Reynolds, N. A. Rayner, T. M. Smith, D. C. Stokes, and W. Q. Wang, Journal of Climate **15**, 1609 (2002).